J|A|C|S
ARTICLES
Published on Web 12/18/2002

Macrocyclic Glycoclusters. Self-Aggregation and Phosphate-Induced Agglutination Behaviors of Calix[4]resorcarene-Based Quadruple-Chain Amphiphiles with a Huge Oligosaccharide Pool

Osamu Hayashida,[‡] Keiji Mizuki,[§] Kazuyuki Akagi,[§] Aki Matsuo,[§] Takuya Kanamori,[†] Takashi Nakai,[†] Shinsuke Sando,[†] and Yasuhiro Aoyama*[,†]

Contribution from the Department of Synthetic Chemistry and Biological Chemistry, Graduate School of Engineering, Kyoto University, Yoshida, Sakyo-ku, Kyoto 606-8501, Japan, Institute for Fundamental Research of Organic Chemistry, Kyushu University, Hakozaki, Higashi-ku, Fukuoka 812-8581, Japan, and Department of Chemistry and Biochemistry, Graduate School of Engineering, Kyushu University, Hakozaki, Higashi-ku, Fukuoka 812-8581, Japan

Received July 4, 2002; E-mail: aoyamay@sbchem.kyoto-u.ac.jp

Abstract: Macrocyclic glycocluster compounds $\mathbf{2}_n$ ($n = 2-7$) with four alkyl (undecyl) chains and eight oligosaccharide moieties on the opposite sides of the calix[4]resorcarene macrocycle are prepared from the reactions of the corresponding octaamine derivative with maltooligosaccharide lactones. Combined evidence from dynamic light scattering (DLS), gel permeation chromatography (GPC), and transmission electron microscopy (TEM) indicates that they form small micelle-like nanoparticles ($d \cong 3$ nm) in water. In the presence of Na_2HPO_4/NaH_2PO_4, nanoparticles are agglutinated with phosphate ions as a glue to grow in size up to 60−100 nm, as revealed by DLS as well as microscopy (TEM and AFM). The phosphate-induced agglutination processes can be followed by surface plasmon resonance (SPR). Amphiphile $\mathbf{2}_n$ is readily immobilized on the hydrophobized sensor chip of SPR to give a closely packed monolayer with oligosaccharide moieties exposed to bulk water. While there is no further adsorption of $\mathbf{2}_n$ on the resulting monolayer, this does occur when the latter is pretreated with the phosphate salts, ultimately giving rise to a multilayer upon repeated treatment of the chip with $\mathbf{2}_n$ and Na_2HPO_4/NaH_2PO_4 in an alternate manner. Kinetic analyses show that the phosphate-mediated inter(saccharide) interactions in terms of rate and affinity are markedly dependent on the oligosaccharide chain lengths (n), becoming more favorable with increasing n's. The novel aggregation and agglutination behaviors observed are discussed in terms of immobilizable and irreversible micelles on the basis of the cone-shaped structure of quadruple-chain amphiphile $\mathbf{2}_n$ having a huge saccharide pool and the efficiency of multiple hydrogen bonding therein. The unique intermolecular binding properties of compound $\mathbf{2}_2$ and analogues so far reported are reviewed in light of the present finding.

Introduction

Cell surfaces are abundant in oligosaccharides. They occur as either glycolipids or glycoproteins and play important roles in triggering nonstationary cell adhesion processes such as fertilization, proliferation, viral/bacterial infection, trapping of leucocytes, and cancer transfer.[1] The interactions of clustering oligosaccharides with their biological receptors are often claimed to be specific and multivalent. The so-called cluster effects[2] have been a subject of considerable studies using artificial multivalent saccharide derivatives such as polymers,[3] dendrons and dendrimers,[4] surfactant aggregates,[5] and self-assembled monolayers on gold nanoclusters.[6] We, on the other hand, introduced macrocyclic glycocluster compounds $\mathbf{2}_n$ (Scheme 1), having four long alkyl (undecyl) chains and eight oligosaccharide moieties on the opposite sides of the calix[4]resorcarene macrocycle.[7,8] Their characteristic structure may be viewed as a covalent bundle of glycolipid mimics.[9] They are monodispersed and capable of unimolecularly forming a glycocluster composed of a definite

[†] Kyoto University.
[‡] Institute for Fundamental Research of Organic Chemistry, Kyushu University.
[§] Graduate School of Engineering, Kyushu University.
* To whom correspondence should be addressed. E-mail: aoyamay@sbchem.kyoto-u.ac.jp.

(1) (a) Hakomori, S. *Pure Appl. Chem.* **1991**, *63*, 473−482. (b) Kobata, A. *Acc. Chem. Res.* **1993**, *26*, 319−324. (c) Hakomori, S. *Glycoconjugate J.* **2000**, *17*, 627−647.
(2) (a) Lee, Y. C.; Townsend, R. R.; Hardy, M. R.; Lonngren, J.; Arnarp, J.; Haraldsson, M.; Lonn, H. *J. Biol. Chem.* **1983**, *258*, 199−202. (b) Lee, Y. C.; Lee, R. T. *Acc. Chem. Res.* **1995**, *28*, 321−327.
(3) (a) Nishimura, S.-I.; Matsuoka, K.; Furuike, T.; Ishii, S.; Kurita, K. *Macromolecules* **1991**, *24*, 4236−4241. (b) Mortell, K. H.; Gingras, M.; Kiessling, L. L. *J. Am. Chem. Soc.* **1994**, *116*, 12053−12054. (c) Lee, W. J.; Spaltenstein, A.; Kingery-Wood, J. E.; Whitesides, G. M. *J. Med. Chem.* **1994**, *37*, 3419−3433. (d) Kobayashi, K.; Tsuchida, A.; Usui, T.; Akaike, T. *Macromolecules* **1997**, *30*, 2016−2020. (e) Choi, S. K.; Mammen, N.; Whitesides, G. M. *J. Am. Chem. Soc.* **1997**, *119*, 4103−4111. (f) Zanini, D.; Roy, R. *J. Org. Chem.* **1998**, *63*, 3486-3491. (g) Matsuura, K.; Tsuchida, A.; Okahata, Y.; Akaike, T.; Kobayashi, K. *Bull. Chem. Soc. Jpn.* **1998**, *71*, 2973−2977. (h) Gordon, E. J.; Gestwicki, J. E.; Strong, L. E.; Kiessling, L. L. *Chem. Biol.* **2000**, *7*, 9−16. (i) Akai, S.; Kajihara, Y.; Nagashima, Y.; Kamei, M.; Arai. J.; Bito, M.; Sato, K. *J. Carbohydr. Chem.* **2001**, *20*, 121−143. (j) Cairon, C. W.; Gestwicki, J. E.; Kanai, M.; Kiessling, L. L. *J. Am. Chem. Soc.* **2002**, *124*, 1615−1619.

10.1021/ja0275663 CCC: $25.00

Scheme 1. Preparation of Glycocluster $\mathbf{2}_n$

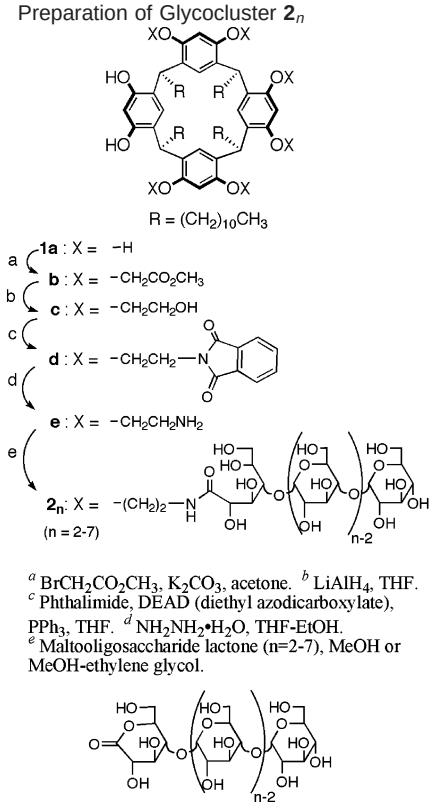

[a] $BrCH_2CO_2CH_3$, K_2CO_3, acetone. [b] $LiAlH_4$, THF. [c] Phthalimide, DEAD (diethyl azodicarboxylate), PPh_3, THF. [d] $NH_2NH_2 \cdot H_2O$, THF-EtOH. [e] Maltooligosaccharide lactone (n=2-7), MeOH or MeOH-ethylene glycol.

number of saccharide moieties in a well-defined geometry. These are apparent merits of such compounds in light of possible complication associated with folding and clustering processess for the glycopolymers and simple glycosurfactants.

Our previous work reveals that compounds $\mathbf{2}_2$ and analogues exhibit a number of unique binding properties in water. One is that of efficient hydrophobic hosts.[7b,i] Another is that of polar adsorbates, being assembled on a polar solid surface such as quartz[7a] and agglutinated with phosphate ions.[7h,j] Still the third is that of selective targets of proteins,[7b] viruses,[7g] and cells[7i] as biological saccharide-receptors. To fully understand these phenomena and to reveal the general and potential utilities of macrocyclic skeletons to put saccharide moieties on, it is essential to elucidate the detailed structural characteristics of bowl-shaped glycoclusters $\mathbf{2}_n$ not only as unimolecular entities but also as self-assembling amphiphiles.[10] As amphiphiles, they have a number of unique aspects. They are nonionic. They are four-legged rather than two-legged as is usually the case in phospholipids and glycolipids. Nevertheless, the oligosaccharide pool as a polar head is unbalancingly huge as compared with the pool as an apolar part. We are concerned here about light scattering, gel permeation, microscopic, and surface plasmon resonance[11] characterization of their assembling properties in water and in phosphate buffer. We report here that they form micelle-like nanoparticles of an unusual stability, which as such are agglutinated with the phosphate ions as a glue.

Results and Discussion

Preparation and Self-Aggregation. Calix[4]resorcarene is a bowl-shaped resorcinol cyclic tetramer with four alkyl tails, R = undecyl[12] in the present case (Scheme 1), which are known to be oriented in the same direction.[13] Reactions of octaamine **1e** with maltooligosaccharide lactones[14] having a glucose chain length of $n = 2-7$ proceed smoothly (yield, 44−76%) to give amide-linked octa(maltooligosaccharide) derivatives $\mathbf{2}_n$ having a huge oligosaccharide cluster part composed of $8n = 16$ (in $\mathbf{2}_2$) to 56 (in $\mathbf{2}_7$) glucose residues, one as a ring-opened linear connector and $(n - 1)$ as an intact pyranose per chain. The molecular weights range from 4172 for $\mathbf{2}_2$ to 10 650 for $\mathbf{2}_7$.

Despite the presence of four long alkyl chains in addition to four benzene rings, compounds $\mathbf{2}_n$ are miscible with water, having a solubility of >1 g/mL, and completely insoluble even in methanol. Furthermore, they are not surface active at least at 1 mM in water as far as surface tensions are concerned.[15] An indication of their amphiphilic nature, on the other hand, comes from their broadened ^1H NMR signals in D_2O. Dynamic light scattering (DLS) in fact reveals that they form small nanoparticles[16] in aqueous media over a wide concentration range, even in a micromolar region. Typical histograms for maltose- and maltopentaose-derived compounds $\mathbf{2}_2$ and $\mathbf{2}_5$ at 0.1 mM are shown in Figure 1a and e, respectively, where the size distribution evaluated by a Marquardt analysis[17] of the data is in reference to the number of particles.[16] The histograms remain the same at least for 2 days at 30 °C. The particles are of a

(4) (a) Roy, R.; Zanini, Meunier, S. J.; Romanowska, A. *J. Chem. Soc., Chem. Commun*. **1993**, 1869−1870. (b) Roy, R.; Park, W. K. C.; Wu, Q.; Wang, S. N. *Tetrahedron Lett.* **1995**, *36*, 4377−4380. (c) Ashton, P. R.; Boyd, S. E.; Brown, C. L.; Jayaraman, N.; Nepogodiev, S. A.; Stoddart, J. F. *Chem.-Eur. J.* **1996**, *2*, 1115−1128. (d) Pavlov, G. M.; Korneeva, E. V.; Jumel, K.; Harding, S. E.; Meijer, E. W.; Peerlings, H. W. I.; Stoddart, J. F.; Nepogodiev, S. A. *Carbohydr. Polym*. **1999**, *38*, 195−202. (e) Fulton, D. A.; Stoddart, J. F. *Org. Lett.* **2000**, *2*, 1113−1116. (f) Aoi, K.; Itoh, K.; Okada, M. *Macromolecules* **1995**, *28*, 531−5393.

(5) (a) Kingery-Wood, J. E.; Williams, K. W.; Sigal, G. B.; Whitesides, G. M. *J. Am. Chem. Soc*. **1992**, *114*, 7303−7305. (b) Zhang, T.; Marchant, R. E. *J. Colloid Interface Sci*. **1996**, *177*, 419−426.

(6) (a) de la Fuente, Barrientos, A. G.; Rojas, T. C.; Rojo, J.; Canãda, J.; Fernández, A.; Penadés, S. *Angew. Chem., Int. Ed.* **2001**, *40*, 2258−2261. (b) Tromas, C.; Rojo, J.; de la Fuente, Barrientos, A. G.; García, R.; Penadés, S. *Angew. Chem., Int. Ed.* **2001**, *40*, 3052−3055.

(7) (a) Fujimoto, T.; Shimizu, C.; Hayashida, O.; Aoyama, Y. *J. Am. Chem. Soc.* **1997**, *119*, 6676−6677. (b) Fujimoto, T.; Shimizu, C.; Hayashida, O.; Aoyama, Y. *Gazz. Chim. Ital.* **1997**, *127*, 749−752. (c) Hayashida, O.; Shimizu, C.; Fujimoto, T.; Aoyama, Y. *Chem. Lett*. **1998**, 13−14. (d) Fujimoto, T.; Shimizu, C.; Hayashida, O.; Aoyama, Y. *J. Am. Chem. Soc.* **1998**, *120*, 601−602. (e) Ariga, K.; Isoyama, K.; Hayashida, O.; Aoyama, Y.; Okahata, Y. *Chem. Lett*. **1998**, 1007−1008. (f) Aoyama, Y.; Matsuda, Y.; Chuleeraruk, J.; Nishiyama, K.; Fujimoto, T.; Fujimoto, K.; Shimizu, T.; Hayashida, O. *Pure Appl. Chem.* **1998**, *70*, 2379−2384. (g) Fujimoto, K.; Hayashida, O.; Aoyama, Y.; Guo, C.-T.; Hidari, K. I.-P. J.; Suzuki, Y. *Chem. Lett.* **1999**, 1259−1260. (h) Hayashida, O.; Kato, M.; Akagi, K.; Aoyama, Y. *J. Am. Chem. Soc.* **1999**, *121*, 11597−11598. (i) Fujimoto, K.; Miyata, T.; Aoyama, Y. *J. Am. Chem. Soc.* **2000**, *122*, 3558−3559. (j) Hayashida, O.; Matsuo, A.; Aoyama, Y. *Chem. Lett.* **2001**, 272−273.

(8) For a calix[4]arene derivative having four side chains with a terminal sugar moiety, see: Marra, A.; Schermann, M.-C.; Dondoni, A.; Casnati, A.; Minari, P.; Ungaro, R. *Angew. Chem., Int. Ed. Engl*. **1994**, *33*, 2479−2481.

(9) A typical class of glycolipids are sphingoglycolipids in which a fatty acid and an oligosaccharide chain are connected to sphingosine, a long-chain amino alcohol, via amide and glycoside linkages, respectively.

(10) For aggregation behaviors of glycolipids and related saccharide-functionalized amphiphiles, see: (a) Fuhrhop, J.-H.; Helfrich, W. *Chem. Rev.* **1993**, *93*, 1565−1582. (b) Vollhardt, D.; Emrich, G.; Gutberlet, T.; Fuhrhop, J.-H. *Langmuir* **1996**, *12*, 5659−5663. (c) Fuhrhop, J.-H.; Bedurke, T.; Gnade, M.; Schneider, J.; Doblhofer, K. *Langmuir* **1997**, *13*, 455−459. (d) Takeoka, S.; Sou, K.; Boettcher, C.; Fuhrhop, J.-H.; Tsuchida, E. *J. Chem. Soc., Faraday Trans.* **1998**, *94*, 2151−2158. (e) Donner, D.; Boettcher, C.; Messerschmidt, C.; Siggel, U.; Fuhrhop, J.-H. *Langmuir* **1999**, *15*, 5029−5039. (f) Li, G.; Fudickar, W.; Skupin, M.; Klyszcz, A.; Draeger, C.; Lauer, M.; Fuhrhop, J.-H. *Angew. Chem., Int. Ed*. **2002**, *41*, 1828−1852.

(11) For a preliminary SPR study on the immobilization of compound $\mathbf{2}_2$ and analogues and binding of polar compounds thereon, see ref 7c.

(12) Aoyama, Y.; Tanaka, Y.; Sugahara, S. *J. Am. Chem. Soc.* **1989**, *111*, 3397−5404.

(13) Böhmer, V. *Angew. Chem., Int. Ed. Engl*. **1995**, *34*, 713−745.

(14) (a) Williams, T. J.; Plessas, N. R.; Goldstein, I. J. *Carbohydr. Res.* **1978**, *67*, C1−C3. (b) Kobayashi, K.; Sumitomo, H.; Ina, Y. *Polym. J.* **1985**, *17*, 567−575.

(15) It is only at $[\mathbf{2}_2] \cong 50$ mM (~20 wt %) when a distinct reduction in surface tension (~40 dyn/cm) is observed. This may be interpreted in terms of bulk effects.

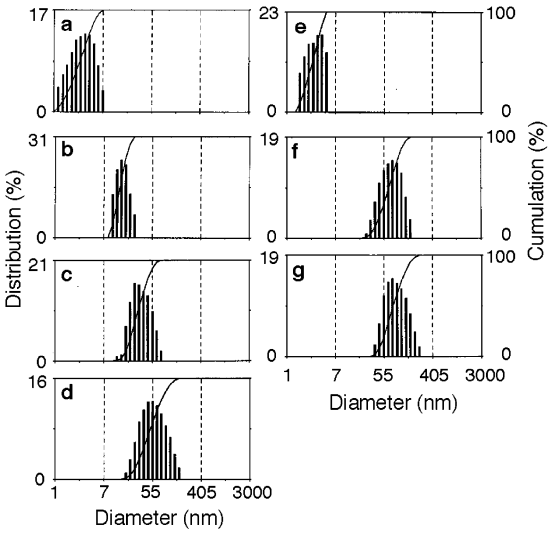

Figure 1. Time courses for the change in size distribution (in reference to number of particles) for aggregates of $\mathbf{2}_2$ (a−d) and $\mathbf{2}_5$ (e−g) in water at 0.1 mM upon addition of Na_2HPO_4/NaH_2PO_4 (100 equiv, keeping the pH of the solution at 7) as evaluated by DLS with a 50 mW Ar^+ laser at 30 °C. Time in h after injection of the phosphate salts: 0 (before injection; a and e), 0.1 (f), 0.5 (b), 7 (g), 44 (c), and 67 (d).

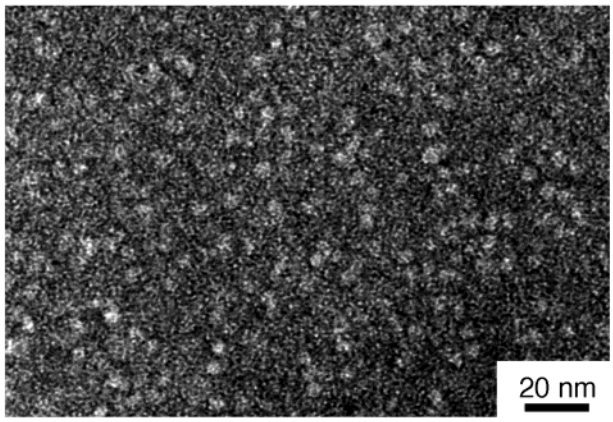

Figure 2. TEM image of the micellar nanoparticles of compound $\mathbf{2}_2$.

micellar size ($d_{mic} = 3.5 \pm 1.1$ nm for $\mathbf{2}_2$ and 3.2 ± 1.1 nm for $\mathbf{2}_5$) and show no notable oligosaccharide chain-length dependence (2.4 ± 0.9 nm for $\mathbf{2}_3$, 2.7 ± 0.9 nm for $\mathbf{2}_4$, and 3.2 ± 1.3 nm for $\mathbf{2}_7$). In Figure 2 is shown a TEM (transmission electron microscopy) image of the nanoparticles (4−6 nm) of compound $\mathbf{2}_2$.

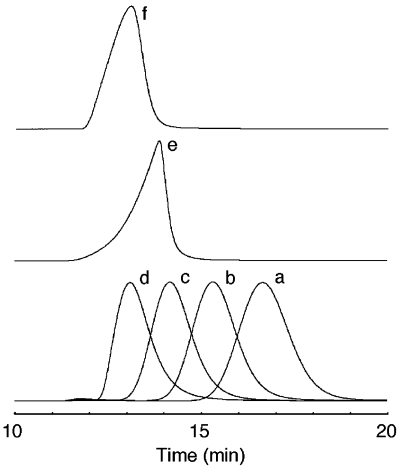

Figure 3. Gel permeation chromatograms for pullulans as calibration standards having molecular weights of 5900 (a), 11 800 (b), 22 800 (c), and 47 300 (d), compound $\mathbf{2}_2$ (e), and compound $\mathbf{2}_7$ (f) with water as an eluant.

Remarkably, the micellar nanoparticles manifest themselves in gel permeation chromatography (GPC).[18] Compounds $\mathbf{2}_2$ (molecular weight, 4172) and $\mathbf{2}_7$ (10 650) are eluted with water exclusively as small aggregates having pullulan-calibrated total molecular weights of 27 000 and 48 000, respectively (Figure 3). These molecular weights indicate that micellar nanoparticles of $\mathbf{2}_2$ and $\mathbf{2}_7$ are composed of ∼6 and ∼4 molecules of amphiphiles $\mathbf{2}_2$ and $\mathbf{2}_7$, respectively.

Phosphate-Induced Agglutination. We have previously shown that glycoclusters $\mathbf{2}_2$ and, in a more pronounced manner, $\mathbf{2}_5$ undergo HPO_4^{2-}-induced agglutination.[7h] This demonstration is based on the ^{31}P NMR titration results and the unusual observations on eventual saccharide-phosphate coprecipitation.[19,20] The agglutination phenomenon can be followed by DLS, TEM, and AFM (atomic force microscopy). In Figure 1 are shown the time courses of the change in the DLS histograms for compounds $\mathbf{2}_2$ (a−d) and $\mathbf{2}_5$ (e−g). Upon addition of Na_2HPO_4/NaH_2PO_4, the small nanoparticles of short-chain amphiphile $\mathbf{2}_2$ rapidly disappear with a compensating appearance of medium-sized aggregates, which further grow in size up to 63 ± 32 nm in 3 days (Figure 1d). In the case of long-chain counterpart $\mathbf{2}_5$, the formation of medium-sized aggregates (99 ± 45 nm, Figure 1g) is more rapid.

The formation of medium-sized $\mathbf{2}_2$-phosphate and $\mathbf{2}_5$-phosphate aggregates is also confirmed by AFM (Figure 4a for $\mathbf{2}_2$-phosphate aggregates with a size of 50−100 nm) and TEM (Figure 4c for $\mathbf{2}_5$-phosphate aggregates with a size of 80−140 nm). The microscopic sizes are in excellent agreement with the

(16) A trace amount of larger assemblies of a vesicular size (280 ± 120 nm for $\mathbf{2}_2$) is also detected in DLS in reference to the intensity of scattered light. According to the theory,[a−c] the intensity-based populations of uniform and spherical particles can be converted to the weight-based and number-based populations by being divided by d^3 and d^6 (d = size (diameter) of the particles), respectively. The observed intensity ratio of the small or micellar nanoparticles (M) to the large or vesicular assemblies (V) for compound $\mathbf{2}_2$ is $I^M/I^V \cong 0.18$. In terms of weight and number, the ratios are $W^M/W^V \cong (I^M/I^V)[(d^V)^3/(d^M)^3] = 0.18 \times (280^3/3.5^3) = 9 \times 10^4$ and $N^M/N^V \cong (I^M/I^V)[(d^V)^6/(d^M)^6] = 0.18 \times (280^6/3.5^6) = 5 \times 10^{10}$, respectively ($d^M = 3.5$ nm and $d^V = 280$ nm). Thus, the number of vesicles is almost completely negligible as compared with that of micelles, as is in fact the case (Figure 1a and e). The weight ratio W^M/W^V reflects the molecular distribution of compound $\mathbf{2}_2$ between micelles and vesicles. Thus, the number of molecules ($\mathbf{2}_2$) involved in vesicles, even when they are supposed to be filled with $\mathbf{2}_2$, is negligible as compared with that contained in micelles. This is also confirmed by GPC.[18] (a) Rayleigh, L. *Proc. R. Soc. London* **1914**, *A90*, 219−225. (b) Flory, P. J. *Principles of Polymer Chemistry*; Cornell University Press: New York, 1953; Chapter 7. (c) Taylor, T. W.; Scrivner, S. M.; Sorensen, C. M.; Merklin, J. F. *Appl. Opt.* **1985**, *24*, 3713−3717.

(17) Norgren, M. *Math. Comput. Simul.* **1999**, *50*, 553−575.

(18) As independently confirmed by DLS measurements, the trace amount of vesicular assemblies can be removed by filtration of the solution of amphiphile $\mathbf{2}_2$ through a membrane filter of 200 nm pores. The chromatogram for the vesicle-free solution thus obtained is the same as that shown in Figure 3, which is actually for an unfiltered solution. Thus, vesicular assemblies if any are only in an undetectable amount, in agreement with the DLS results in reference to the weight- or number-based population.

(19) For the hydrogen-bonded saccharide-phosph(on)ate complexes in organic media, see: (a) Das, G.; Hamilton, A. D. *J. Am. Chem. Soc.* **1994**, *116*, 11139−11140. (b) Anderson, S.; Neidlein, U.; Gramlich, V.; Diederich, F. *Angew. Chem., Int. Ed. Engl.* **1995**, *34*, 1596−1599. (c) Coterón, J. M.; hacket, F.; Schneider, H.-J. *J. Org. Chem.* **1996**, *61*, 1429−1435. (d) Das, G.; Hamilton, A. D. *Tetrahedron Lett.* **1997**, *38*, 3675−3678. (e) Dondoni, A.; Marra, A.; Schermann, M.-C.; Casnati, A.; Sansone, F.; Ungaro, R. *Chem.-Eur. J.* **1997**, *3*, 1774−1782.

(20) For the complexation of polysaccharides and nucleic acids, see: (a) Sakurai, K.; Shinkai, S. *J. Am. Chem. Soc.* **2000**, *122*, 4520−4522. (b) Sakurai, K.; Mizu, M.; Shinkai, S. *Biomacromolecules* **2001**, *2*, 641−650.

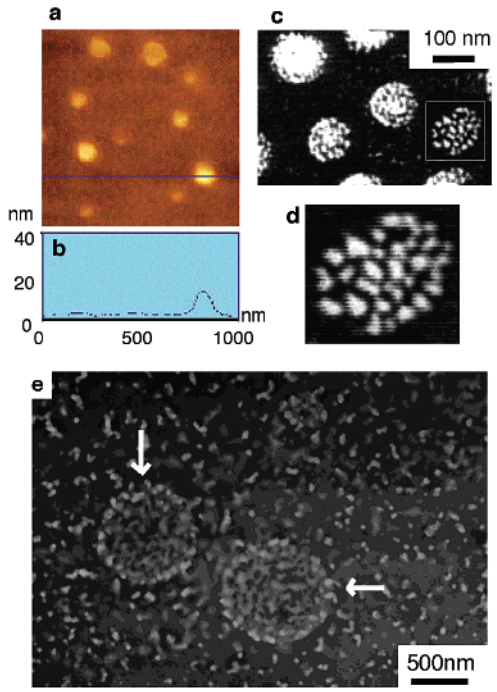

Figure 4. Micrographs for medium-sized aggregates formed from phosphate-induced agglutination of amphiphiles $\mathbf{2}_2$ and $\mathbf{2}_5$ after centrifugation: AFM image of the $\mathbf{2}_2$-phosphate aggregates on a mica plate (a) and its cross section (b), TEM image of the $\mathbf{2}_5$-phosphate aggregates (c) and an enlargement of an aggregate (d), and TEM image of a dynamic $\mathbf{2}_2$-phosphate agglutination process taken immediately after sonication (e), the arrows being where small particles are gathering to form a larger aggregate.

Scheme 2. Self-Aggregation and Phosphate-Induced Agglutination of Amphiphile $\mathbf{2}_n$

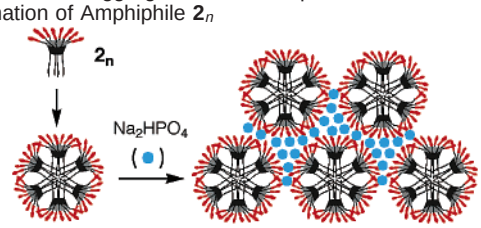

DLS sizes. A cross section of the AFM topographies shows a convex top surface (Figure 4b), suggesting that the aggregates have no internal water pool. The TEM image (Figures 4c and its enlargement 4d) reveals that the aggregates are composed of smaller particles whose size (several nanometers) corresponds to that of micellar nanoparticles. This is confirmed also dynamically by the TEM photograph (Figure 4e) taken immediately after sonication of a solution of compound $\mathbf{2}_2$ and Na_2HPO_4/NaH_2PO_4, where small nanoparticles are clearly shown to be assembling to form larger aggregates, as shown by the arrows. These results, coupled with the above DLS observations, leave little doubt that the phosphate-induced agglutination of amphiphiles $\mathbf{2}_2$ and $\mathbf{2}_5$ is actually phosphate-mediated cross-linking of micellar nanoparticles, as shown in Scheme 2 in the next paragraph.

Micellar Nanoparticles. The nanoparticles in concern may be formed in an usual manner in which conventional amphiphilic surfactants are micellized, where entangling alkyl chains form a hydrophobic core and polar headgroups exposed to bulk water define a spherical surface. Nevertheless, the formation of "micelles" from four-legged or quadruple-chain amphiphile $\mathbf{2}_n$ may appear somehow curious in view of a general tendency of

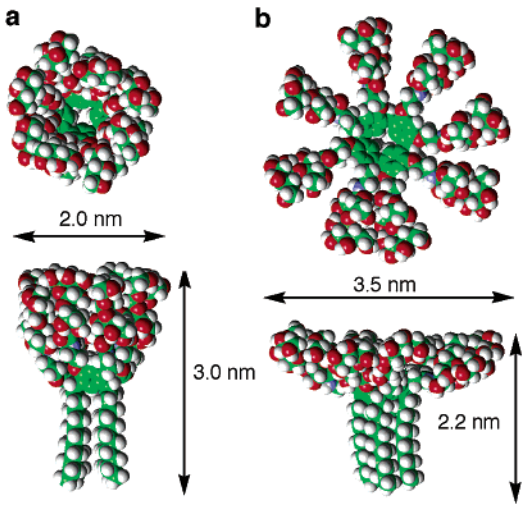

Figure 5. Space-filling top view (top) and side view (bottom) of compound $\mathbf{2}_2$ with its glycocluster portion in the folded (a) or unfolded (b) conformation. Carbon, hydrogen, oxygen, and nitrogen atoms are shown in green, white, red, and blue, respectively.

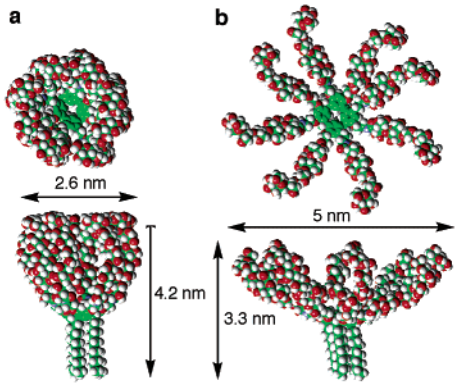

Figure 6. Space-filling top view (top) and side view (bottom) of compound $\mathbf{2}_5$ with its glycocluster portion in the folded (a) or unfolded (b) conformation. Carbon, hydrogen, oxygen, and nitrogen atoms are shown in green, white, red, and blue, respectively.

single- and double-chain amphiphiles to form micelles and bilayers such as vesicles and lamellae,[21] respectively. In Figures 5 and 6 are shown the space-filling CPK models (top views (top) and side views (bottom)) with estimated molecular dimensions for compounds $\mathbf{2}_2$ and $\mathbf{2}_5$, respectively. The bowl-shaped calix[4]resorcarene platform with four undecyl chains sustains a glycocluster composed of 16 (in $\mathbf{2}_2$) or 40 (in $\mathbf{2}_5$) monosaccharide residues in a conformation which can span from folded or compact (a) to unfolded or extended (b), depending on the extents to which oligosaccharide chains are intramolecularly packed. Evidently, the clustering oligosaccharide moieties as a polar head even in the folded conformation of $\mathbf{2}_2$ (Figure 5a) is unbalancingly huge as compared with the clustering of the apolar portion. Lateral packing of such a cone-shaped amphiphile, especially in the unfolded conformation, necessarily generates curvature, a situation suited for forming spherical micelles. This must be the case for the formation of the present micellar nanoparticles (Scheme 2, where amphiphile $\mathbf{2}_n$ is shown in a schematic form), whose size (3.5 nm for $\mathbf{2}_2$ by DLS) is reasonable in light of the molecular height of constituent

(21) (a) Kunitake, T.; Okahata, Y.; Shimomura, M.; Yasunami, S.; Takarabe, K. *J. Am. Chem. Soc.* **1981**, *103*, 5401−5413. (b) Kunitake, T. *Angew. Chem., Int. Ed. Engl.* **1992**, *31*, 709−726.

amphiphile $\mathbf{2}_2$ (Figure 5). Also reasonable are the GPC-evaluated aggregation numbers of 6 and 4, respectively, for the $\mathbf{2}_2$- and $\mathbf{2}_7$-derived nanoparticles. A rough surface-area calculation, for example, indicates that each molecule of $\mathbf{2}_2$ has an occupation area of 6 nm^2 on the micellar surface.[22] This is between the surface area (3 nm^2) of the glycocluster part of molecule $\mathbf{2}_2$ in the folded conformation (Figure 5a) and that (10 nm^2) in the unfolded conformation (Figure 5b).[22] It is likely that the glycocluster moiety of $\mathbf{2}_2$ in the micelles is in a more or less unfolded form so as to allow intermolecular interactions of the oligosaccharide chains.

Micelles are usually in equilibrium with constituent monomers. This is, however, not a practical picture of the present system which is essentially irreversible. Thus, amphiphile $\mathbf{2}_2$, which forms micellar nanoparticles in a micromolar range, shows no surface activity even in a micromolar range, indicating that there is no equilibrium dissociation of a particle into monomers. This is also why the present micellar nanoparticles can be detected as such in GPC; micelles, in contrast to vesicles, cannot usually retain integrity as such under GPC conditions. Micelles are usually too dynamic to be frozen. In a marked contrast, the present nanoparticles are readily immobilized upon phosphate coating.

The irreversible micellization could not readily be understood in terms of hydrophobic driving forces alone, even when the multiple hydrophobic association involving the four alkyl chains in the present system is efficient. There seems to be another source of extra stabilization of the present micelles. A candidate, although by no means convincing, is lateral or side-by-side intermolecular saccharide−saccharide interactions on the micellar surface, as suggested above. There is, however, no indication of front-to-front inter(saccharide) interactions that would lead to self-aggregation of the micellar particles. The phosphate-mediated cross-linking of otherwise nonadhesive saccharide-covered nanoparticles strongly suggests that the phosphate ions and the oligosaccharide chains serve as a glue and a tab for sticking, respectively. The apparent chain-length dependence, that is, readier agglutination of $\mathbf{2}_5$ over $\mathbf{2}_2$, further supports the view, as is discussed in more detail in the following section.

The previous ^{31}P NMR study shows that what is responsible for the Na_2HPO_4/NaH_2PO_4-induced agglutination of $\mathbf{2}_2$ and $\mathbf{2}_5$ is not the sodium ions but the phosphate dianions (HPO_4^{2-}), which undergo partial protonation with the glycoclusters in a reversible manner.[7h] The present picture of the agglutination reinforces the view that the otherwise inefficient hydrogen bonding in water becomes so effective between clustering oligosaccharide moieties with many OH groups as H-donors and multivalent phosphate dianions as H-acceptors. The entangling saccharide chains may form an intramolecular/intermolecular/interparticle oligosaccharide pool, in which a huge number (judging from the stoichiometry of agglutination of $\mathbf{2}_2$: phosphate $\cong$ 1:50)[7h] of sodium phosphate salts are effectively extracted or solubilized. It is remarkable that simple salts which are otherwise soluble only in water are better microsolvated in the saccharide pool than in bulk water.

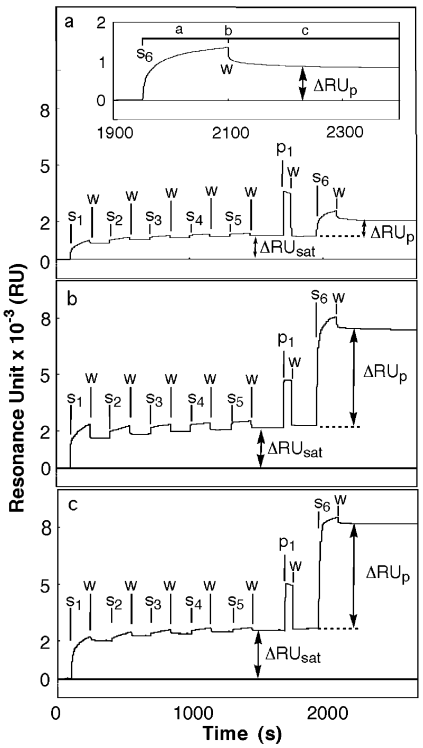

Figure 7. SPR response curves for the immobilization of amphiphile $\mathbf{2}_n$ (n = 2 (a), 5 (b), and 7 (c)) on a hydrophobized sensor chip (step s_n/w; n = 1−5), phosphate coating (step p_1/w), and further adsorption of $\mathbf{2}_n$ on the resulting phosphate-covered monolayer $\mathbf{2}_n$ (step s_6/w) in the flow of water at a flow rate of 10 μL/min. Steps s, p, and w stand for an injection of an aqueous solution of analyte $\mathbf{2}_n$ (0.2 mM, 25 μL), that of Na_2HPO_4/NaH_2PO_4 (0.1 M at pH 7, 10 μL), and water (31 μL), respectively. Inset: enlargement of the s_6/w process for $\mathbf{2}_2$.

SPR Characterization. Surface plasmon resonance (SPR) is a kind of gravimetry applicable to adsorption phenomena.[23] If something is bound to an SPR sensor chip, a change is induced in reflective index in the vicinity of the surface. This is detected as a change in the intensity of light in the form of resonance unit (*RU*).[24] We use here a hydrophobized sensor chip (HPA),[11] whose Au surface is coated with long-chain alkanethiol molecules via S−Au bonds. The actual operation of SPR consists of an injection of a solution of analyte or adsorbate (step s) followed by that of a running solvent water (step w). Repeated treatment of the chip with saccharide amphiphile $\mathbf{2}_2$ (a), $\mathbf{2}_5$ (b), or $\mathbf{2}_7$ (c) (steps s_1/w−s_5/w) results in an increase in *RU* until saturation is reached as shown in Figure 7. Using the known relationship between ΔRU and the amount of analyte adsorbed,[25] we converted the saturation values observed (ΔRU_{sat}) into the packing densities (P) and hence the occupation areas (A) for the adsorbates $\mathbf{2}_2$, $\mathbf{2}_5$, or $\mathbf{2}_7$ at saturation binding, as summarized in Table 1. The occupation areas increase in the $\mathbf{2}_n$ family with increasing chain lengths from 4.6 for $\mathbf{2}_2$ through

(22) The surface area of $\mathbf{2}_2$-derived spherical micellar nanoparticles having a radius r_{mic} is $S_{mic} = 4\pi r_{mic}^2 = 38.5$ nm^2, where $r_{mic} = 1.75$ nm is taken from the DLS size (diameter) of the particles (3.5 nm for $\mathbf{2}_2$). The occupation area for each molecule of $\mathbf{2}_2$ in a micelle is $S = S_{mic}/n_{agg} = 38.5/6 \cong 6$ nm^2, where n_{agg} is the aggregation number. The area of the glycocluster part of molecule $\mathbf{2}_2$ in the folded conformation (Figure 5a, d = 2 nm, and hence r = 1 nm) is $S_{fold} = \pi r^2 \cong 3$ nm^2, and that in the unfolded conformation (Figure 5b, d = 3.5 nm, and hence r = 1.75 nm) is $S_{unfold} = \pi r^2 \cong 10$ nm^2.

(23) (a) Shinohara, Y.; Kim, F.; Shimizu, M.; Goto, M.; Tosu, M.; Hasegawa, Y. *Eur. J. Biochem.* **1994**, *223*, 189−194. (b) Mrksich, M.; Sigal, G. B.; Whitesides, G. M. *Langmuir* **1995**, *11*, 4383−4385. (c) Sigal, G. B.; Bamdad, C.; Barberis, A.; Strominger, J.; Whitesides, G. M. *Anal. Chem.* **1996**, *68*, 490−497.

(24) Karlsson, R.; Fält, A. *J. Immunol. Methods* **1997**, *200*, 121−133.

(25) Stenberg, E.; Persson, B.; Roos, H.; Urbaniczky, C. *J. Colloid Interface Sci.* **1991**, *143*, 513−526.

Scheme 3. Hydrophobic Immobilization of Amphiphile $\mathbf{2}_n$ on a Hydrophobized Sensor Chip of SPR and Subsequent Multilayer Formation Mediated by the Phosphate Ions

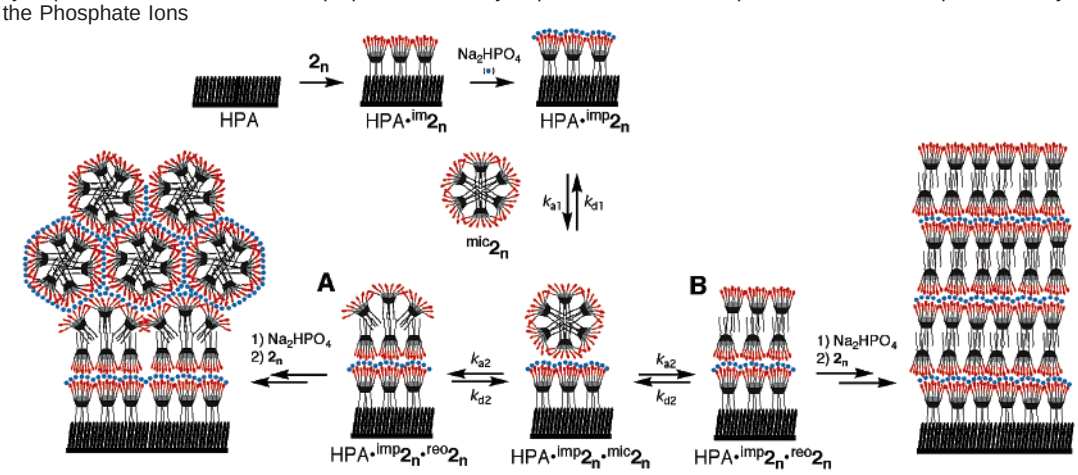

Table 1. Increases in Resonance Unit (ΔRU_{sat}), Packing Densites (*P*), and Occupation Areas (*A*) for the Immobilization of Amphiphiles $\mathbf{2}_2$, $\mathbf{2}_5$, and $\mathbf{2}_7$ at Saturation Binding on a Hydrophobized Sensor Chip of SPR, and Estimated Diameter (*d*) of the Glycocluster Part of $\mathbf{2}_n$ in the Folded Conformation (Refer to Figures 5a and 6a)

compd	ΔRU_{sat}	*P* (molecules/nm^2)	*A* (nm^2/molecule)	*d* (nm)
$\mathbf{2}_2$	1500	0.22	4.6	2.0
$\mathbf{2}_5$	2200	0.16	6.3	2.6
$\mathbf{2}_7$	2500	0.14	7.1	2.8

6.3 for $\mathbf{2}_5$ to 7.1 nm^2/molecule for $\mathbf{2}_7$. They are very close to the estimated cross-sectional areas for the glycocluster moieties in the folded form (Figures 5a and 6a) having a diameter (*d*) shown in Table 1. These results indicate that compounds $\mathbf{2}_n$ are readily immobilized on the chip (HPA), forming a closely packed monolayer (HPA•$^{im}\mathbf{2}_n$) with their alkyl tails embedded in the hydrophobized surface of the chip and their glycocluster moieties, in a folded, unfolded, or intermediate conformation,[26] exposed to the bulk water phase, as schematically shown in Scheme 3.[27,28] The immobilization of the present quadruple-chain amphiphiles is practically irreversible, because they cannot be desorbed unless washed with an aqueous solution of surfactant such as octyl β-D-glucopyranoside.

The formation of monolayer at saturation binding confirms again that there is no efficient multilayer-forming saccharide−saccharide interaction[29,30] even between monolayer and nanoparticle in the present case. However, when treated with an aqueous solution of Na_2HPO_4/NaH_2PO_4 (step p_1/w),[31] phosphate-coated monolayer $\mathbf{2}_n$ (HPA•$^{imp}\mathbf{2}_n$) does bind compound $\mathbf{2}_n$ again as an adsorbate (step s_6/w) (Figure 7a, b, and c for $\mathbf{2}_2$, $\mathbf{2}_5$, and $\mathbf{2}_7$, respectively). The amount of $\mathbf{2}_2$ bound in this way (ΔRU_p) is comparable to that needed for monolayer formation (ΔRU_{sat}) ($\Delta RU_p/\Delta RU_{sat} = 0.8$, Figure 7a), while ΔRU_p is twice or more as much as ΔRU_{sat} in the case of long-chain compounds $\mathbf{2}_5$ and $\mathbf{2}_7$ ($\Delta RU_p/\Delta RU_{sat} = 2.4$ for $\mathbf{2}_5$ and 2.3 for $\mathbf{2}_7$, Figure 7b and c).[32] It is also readily shown that the newly formed surface has saccharide moieties exposed to bulk water, because repeated treatment of the chip with $\mathbf{2}_2$ as an adsorbate and phosphate as a glue[31] in an alternate manner results in multilayer formation (Figure 8).[33]

Two models are conceivable (Scheme 3). A nanoparticle model (A) supposes that micellar nanoparticles in solution are adsorbed essentially as such on the surface and further form a multilayer with such particles as a packing unit as in the case of the in-solution agglutination. A bilayer model (B), on the other hand, assumes that nanoparticles adsorbed on the surface are converted to a bilayer and further form a multilayer with bilayers as a repeating unit. The two models are not distinguishable by SPR.[32]

(26) Any unfolded conformation could also account for the calculated surface if intermolecular interpenetration of the oligosaccharide moieties is allowed.

(27) For examples of SPR studies on glycocluster compounds, see: (a) MacKenzie, C. R.; Hirama, T.; Lee, K. K.; Altman, E.; Young, N. M. *J. Biol. Chem.* **1997**, *272*, 5533−5538. (b) Matsuura, K.; Kitakouji, H.; Sawasa, N.; Ishida, H.; Kiso, M.; Kitajima, K.; Kobayashi, K. *J. Am. Chem. Soc.* **2000**, *122*, 7406−7407. (c) Rathore, D.; McCutchan, T. F.; Garboczi, D. N.; Toida, T.; Hernaiz, M. J.; LeBrun, L. A.; Lang, S. C. *Biochemistry* **2001**, *40*, 11518−11524. (d) Haseley, S. R.; Vermeer, H. J.; Kamerling, J. P.; Vliegenthart, J. F. G. *Proc. Natl. Acad. Sci. U.S.A.* **2001**, *96*, 9419−9424. (e) Hernáiz, M. J.; de la Fuente, J. M.; Barrientos, Á. G.; Penadés, S. *Angew. Chem., Int. Ed.* **2002**, *41*, 1554−1557.

(28) For monolayers of calix[4]resorcarene derivatives formed on solid supports, see: (a) Adams, H.; Davis, F.; Stirling, C. J. M. *J. Chem. Soc., Chem. Commun.* **1994**, *21*, 2527−2529. (b) Thoden van Verzen, E. N.; Engbersen, J. F. J.; de Lange, P. J.; Mahy, J. W. G.; Reinhoudt, D. N. *J. Am. Chem. Soc.* **1995**, *117*, 6853−6862. (c) Schoenherr, H.; Vancso, G. J.; Huisman, B.; Frank, C. J. M.; Reinhoudt, D. N. *Langmuir* **1997**, *13*, 1567−1570. (d) Ueda, M.; Fukushima, N.; Kudo, K.; Ichimura, K. *J. Mater. Chem.* **1997**, *7*, 641−645. (e) Hayashi, Y.; Suzuki, S.; Ichimura, K. *J. Mater. Chem.* **2001**, *11*, 1805−1811.

(29) For biorelevant carbohydrate−carbohydrate interactions, see: (a) Eggens, I.; Fendersen, B.; Toyokuni, T.; Dean, B.; Stroud, M.; Hakomori, S. *J. Biol. Chem.* **1989**, *264*, 9476−9484. (b) Kojima, N.; Hakomori, S. *J. Biol. Chem.* **1989**, *264*, 20159−20162. (c) References 27b,d,e.

(30) For carbohydrate−carbohydrate interactions in artificial host−guest systems, see: (a) Kikuchi, Y.; Tanaka, Y.; Sutarto, S.; Kobayashi, K.; Toi, H.; Aoyama, Y. *J. Am. Chem. Soc.* **1992**, *114*, 10302−10306. (b) Coterón, J. M.; Vicent, C.; Bosso, C.; Penadés, S. *J. Am. Chem. Soc.* **1993**, *115*, 10066−10076. (c) Jiménez-Barbero, J.; Junquera, E.; Martín-Pastor, M.; Sharma, S.; Vicent, C.; Penadés, S. *J. Am. Chem. Soc.* **1995**, *117*, 11198−11204.

(31) Treatment with Na_2HPO_4/NaH_2PO_4 (steps p_1/w in Figure 7 and p_1/w−p_5/w in Figure 8) actually results in no detectable increase in *RU*. This may be due to low SPR sensitivity of sodium phosphate in terms of mass (low molecular weight) as well as reflective index (high polarity).

(32) The amount of $\mathbf{2}_n$ adsorbed (ΔRU_p) as $^{reo}\mathbf{2}_n$ (Scheme 3, as either nanoparticle or bilayer) could be related to the amount of $\mathbf{2}_n$ immobilized (ΔRU_{sat}) as $^{im}\mathbf{2}_n$ and $^{reo}\mathbf{2}_n$ is assumed. On this ground, $\Delta RU_p/\Delta RU_{sat} = 2$ for the bilayer-on-monolayer model B. For the nanoparticle-on-monolayer model A, the ratio $\Delta RU_p/\Delta RU_{sat}$ reflects the ratio of the surface area to the cross-sectional area of the particle, that is, $\Delta RU_p/\Delta RU_{sat} = 4\pi r^2/\pi r^2 = 4$($r$ = radius of the particle). If we take the packing densities for $^{im}\mathbf{2}_n$ (Table 1) and those for the nanoparticles, calculated from their size and aggregation number (3.5 and 6 nm and 3.2 and 4 nm for $\mathbf{2}_5$- and $\mathbf{2}_7$-derived ones, respectively), the ratios would be 2.8 and 3.6 for $\mathbf{2}_5$ and $\mathbf{2}_7$, respectively. Actually, $\Delta RU_p/\Delta RU_{sat} = 0.8$ for $\mathbf{2}_2$, 2.4 for $\mathbf{2}_5$, and 2.3 for $\mathbf{2}_7$ (Figure 7a−c, respectively). Thus, both models A and B are roughly consistent with the experimental results for the long-chain compounds $\mathbf{2}_5$ and $\mathbf{2}_7$. For the short-chain analogue $\mathbf{2}_2$, on the other hand, there might be some defect in close packing of $^{reo}\mathbf{2}_2$.

(33) Ready binding of concanavaline A, a glucose-binding (as well as mannose-binding) lectin, to the surface can be taken as another evidence for the saccharide-coated nature of the latter.

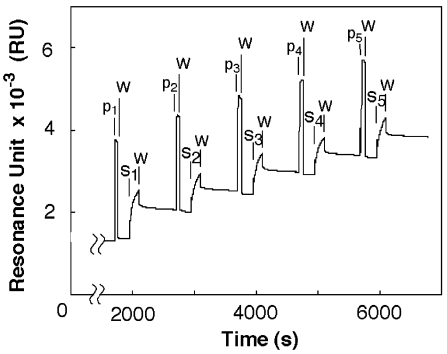

Figure 8. SPR response curves for the phosphate-mediated multilayer formation for amphiphile $\mathbf{2}_2$ (step p_n/w/s_n/w; $n = 1-5$) on a $\mathbf{2}_2$-immobilized sensor chip in the flow of water at a flow rate of 10 μL/min. Steps p, s, and w stand for an injection of an aqueous solution of Na_2HPO_4/NaH_2PO_4 (0.1 M at pH 7, 10 μL), that of analyte $\mathbf{2}_2$ (0.2 mM, 25 μL), and water (31 or 100 μL), respectively.

Table 2. Rate Constants (k_{a1}, k_{d1}, k_{a2}, and k_{d2}, Referring to Scheme 3), Maximal Analyte Binding Capacities (ΔRU_{max}), and Affinity Constants (K) Associated with the Binding of Analyte $\mathbf{2}_n$ on the Phosphate-Coated Monolayer $\mathbf{2}_n$ Immobilized on a Sensor Chip

monolayer	analyte	k_{a1} ($M^{-1}\,s^{-1}$)	k_{d1} (s^{-1})	k_{a2} (s^{-1})	k_{d2} (s^{-1})	ΔRU_{max}	K (M^{-1})
$\mathbf{2}_2$	$\mathbf{2}_2$	190	0.024	0.016	2.2×10^{-4}	1280	4.4×10^5
$\mathbf{2}_5$	$\mathbf{2}_5$	510	0.026	0.024	7.2×10^{-5}	5470	6.4×10^6
$\mathbf{2}_7$	$\mathbf{2}_7$	450	0.0049	0.021	1.5×10^{-5}	5650	1.3×10^8

Chain-Length Dependence. An SPR response curve consists of three parts, a rising curve (a) starting with an injection of analyte (adsorbate), a sharp drop in *RU* gained (b) upon addition of running solvent water, and a subsequent declining curve (c), as shown in the inset of Figure 7a for the binding of analyte $\mathbf{2}_2$ on the phosphate-coated monolayer $\mathbf{2}_2$ (HPA·$^{imp}\mathbf{2}_n$, referring to Scheme 3). They represent the increase in [$\mathbf{2}_2$] on the surface of the sensor mainly due to adsorption, elution of nonadsorbed $\mathbf{2}_2$, and desorption of $\mathbf{2}_2$ bound, respectively. In many cases, especially those involving a complicated analyte such as proteins, adsorption and desorption curves are best analyzed on the basis of a two-state model, which involves a conformational change in the analyte adsorbed. This is also the case here. The two-state model gives much better curve fitting with root means squares of RMS = 60−180 than the simple (one-conformation) model with RMS = 390−1880 and is compatible with both models A and B (Scheme 3). Thus, analyte $\mathbf{2}_n$ as a micellar nanoparticle ($^{mic}\mathbf{2}_n$) is adsorbed on the phosphate-coated monolayer surface (HPA·$^{imp}\mathbf{2}_n$) with association and dissociation rate constants k_{a1} and k_{d1}, respectively. The nanoparticles thus adsorbed undergo a reorientation ($^{mic}\mathbf{2}_n \rightarrow {}^{reo}\mathbf{2}_n$) so as to adjust itself to a planar saccharide monolayer platform (model A) or to give a bilayer (model B) with forward and backward rate constants k_{a2} and k_{d2}, respectively. Respective $\mathbf{2}_n$-normalized rate constants evaluated by a computer-aided curve-fitting method, maximal analyte-binding capacities (ΔRU_{max}), and the apparent affinity constants ($K = (k_{a1}/k_{d1})\cdot(k_{a2}/k_{d2})$) are summarized in Table 2. A chain-length dependence is evident. On going from $\mathbf{2}_2$ through $\mathbf{2}_5$ to $\mathbf{2}_7$, there is in each step an increase in K approximately by an order of magnitude, where the decrease in dissociation rate constants (k_{d1} and k_{d2}) plays a more important role than the increase in association rate constants (k_{a1} and k_{a2}).

Nanoparticles in Intermolecular Interactions. An earlier indication of efficient hydrogen bonding involving glycocluster $\mathbf{2}_2$ comes from its ready adsorption on the quartz surface.[7a] As far as packing densities are concerned, the adsorption on the quartz turns out to be similar to that on the SPR sensor chip; the former may also be understood on the basis of model A or B (Scheme 3).

Compound $\mathbf{2}_2$ and its galactose analogue are excellent hosts for hydrophobic guests in water with the binding constants on the order of 10^5-10^6 M^{-1}.[7b,i] The host:guest stoichiometry of 1:1 strongly suggests that the guest-binding site is not the hydrophobic micellar interior but the bowl-shaped metacyclophane cavity of respective host molecules. A question has been what role the clustering oligosaccharide chains have, which in the folded conformation could even block the binding site. It is now likely that the cavity is open because micellization involves the host molecules in a more or less unfolded conformation so as to maximize intermolecular lateral inter(saccharide) interactions.

The galactose-cluster compound is specifically captured by the liver cells via saccharide−receptor interactions, thus delivering included guest molecules to the cells.[7i] The cell specificity actually arises from prohibition of nonspecific adsorption, which is hydrophobic in nature. The masked hydrophobicity of the host parallels the inability of glucose compound $\mathbf{2}_2$ to be in the monomeric state and may be commonly explained in terms of irreversible micellization.

Concluding Remarks

This work reveals the aggregation behaviors of a novel quadruple-chain amphiphile having a huge saccharide pool as a polar head. Because of its characteristic structural feature, compound $\mathbf{2}_n$ forms micellar nanoparticles of masked hydrophobicity in solution or a closely packed monolayer on a hydrophobized solid surface essentially in an irreversible manner. The oligosaccharide moieties alone on the micellar or monolayer surface are not adhesive but act as a tab for sticking and become highly adhesive in the presence of phosphate ions as a glue. The work presents an example of immobilizable micelles, demonstrates the efficiency of multiple hydrogen bonding even in water, affords a visual (microscopic) view of saccharide-triggered adhesion processes, and explains why and how compound $\mathbf{2}_n$ and analogues behave uniquely. However, the real significance of the work we believe is that it shows for the first time how fruitfully the present type of macrocyclic glycoclusters can be used in the study of the multivalency (cluster) effects of saccharides in complexation, recognition, and adhesion.

Experimental Section

Maltooligosaccharide Lactones. Maltooligosaccharides with a chain length of 2−7, that is, maltose, maltotriose, -tetraose, -pentaose, -hexaose, and -heptaose, were readily oxidized with I_2 (4 equiv) in a methanol solution of KOH (4%) containing a minimal amount of water at 40 °C to the corresponding lactones in a yield of >50%, according to the literature for the short-chain derivatives.[14] The carboxylate salts as initial products were recovered by filtration, washed repeatedly with cold methanol and ether, dried, taken in water, and, upon treatment

with an ion-exchange resin in the H^+ form (Amberlite IR-120B), converted to the carboxylic acids, which were taken in methanol or ethanol and evaporated. This procedure of dissolution in alcohol followed by evaporation was repeated approximately 20 times until the materials became completely methanol-soluble, thereby converting the carboxylic acids to the lactones.

Glycocluster Compounds 2_n. Full details for the preparation of octaamine **1e** (Scheme 1) were published elsewhere.[7b] The reaction of **1e** with maltooligosaccharide lactone with glucose residues of ≤4 was carried out in methanol, as illustrated for the preparation of $\mathbf{2}_2$. A solution of octaamine **1e** (0.70 g, 0.48 mmol) in dry methanol (20 mL) was added to a dry methanol solution of maltose-derived lactone (maltonolactone; 2.0 g, 5.8 mmol), and the mixture was stirred at 60 °C for 6 h and cooled to room temperature. The precipitates which separated were collected by filtration, washed with methanol, dried in vacuo, and taken in water. Insoluble materials were removed by filtration, and the filtrate was evaporated to dryness in vacuo to give compound $\mathbf{2}_2$ (1.55 g, 76%) as a white solid: mp 118−120 °C (dec). IR (KBr disk): 1640 cm^{-1} (C═O). ^1H NMR (D_2O): δ 0.81 (t, CH_3), 1.2 (m, $CH_2(CH_2)_9CH_3$), 1.7 (m, $CH_2(CH_2)_9CH_3$), 3−5 (m, O−CH and N−CH), 5.1 (m, Ar−CH), 5.3 (m, anomeric-H), 6.3 and 6.6 (both br s, Ar−H). ^1H NMR (DMSO-d_6): δ 7.83 (br s, NH) in addition to other resonances found for solution in D_2O. Anal. Calcd for $C_{184}H_{312}N_8O_{96}$: C, 52.97; H, 7.54; N, 2.69. Found: C, 52.91; H, 7.66; N, 2.87. The reaction of **1e** with maltooligosaccharide lactone with glucose residues of ≥5 was carried out in a mixture of methanol and ethylene glycol (10/1). Compound $\mathbf{2}_5$ as a representative example: yield 61%; mp 176−181 °C (dec). Anal. Calcd for $C_{328}H_{552}N_8O_{216}\cdot 2H_2O$: C, 48.64; H, 6.92; N, 1.38. Found: C, 48.40; H, 6.98; N, 1.55.

General Measurements. IR and ^1H NMR spectra were obtained on a Shimadzu FTIR-8600PC spectrophotometer and a Bruker DRX600 spectrometer, respectively. Surface tensions on the Whilhelmy principle were taken with a Shimadzu ST-1 surface tensometer. Gel permeation chromatography (GPC) was performed on a Showa Denko Shodex GPC-101 chromatograph using a Shodex Asahipak GS-320 HQ packed column. Molecular weights were calibrated with pullulan standards having a molecular weight of 5900, 11 800, 22 800, or 47 300. Dynamic light scattering (DLS) was carried out for solutions 0.1−1.0 mM in $\mathbf{2}_n$ with or without Na_2HPO_4/NaH_2PO_4 (0.1 M at pH 7) with a Photal dynamic scattering spectrophotometer DLS-7000DL (50 mW Ar^+ laser at 488 nm). TEM (transmission electron microscopy) images of $\mathbf{2}_2$ were taken for a 1.0 mM solution in water with uranyl acetate (2 wt %) as a negative stainer on JEOL JEM-1230 electron microscope at an acceleration voltage of 100 kV. TEM and AFM (atomic force microscopy) photographs of the phosphate aggregates were obtained with a Hitachi H-7500 electron microscope at 100 kV and a TopoMetrix Explorer atomic force microscope, respectively. A solution 6 mM (TEM) or 0.1 mM (AFM) in $\mathbf{2}_n$ with Na_2HPO_4/NaH_2PO_4 (0.1 M at pH 7) in the presence (TEM) or absence (AFM) of phosphotungstic acid (5 wt %) was incubated at 25 °C for 3 min and centrifuged if necessary to remove phosphate-caused turbidity/precipitates. A drop of the resulting clear solution was applied onto a carbon-coated copper grid (TEM) or a mica plate (AFM), and excess solution was removed with the help of filter paper. The grid or plate was kept in vacuo for 1 h to evaporate the solvent and then subjected to the measurements of microscopic images. Surface plasmon resonance (SPR) response curves were recorded on a BIAcore X system docked with a hydrophobized (HPA) sensor chip under the flow of degassed water (10 μL/min). The chip was perfused overnight with degassed water and then washed with an aqueous solution of octyl β-D-glucopyranoside (40 mM, 15 μL) just prior to immobilization of compound $\mathbf{2}_n$.

Kinetic Analysis. The kinetic analysis of the association/dissociation of amphiphile $\mathbf{2}_n$ (n = 2, 5, or 7) on/from the phosphate-coated monolayer (HPA·$^{imp}\mathbf{2}_n$) on the sensor chip (s_6/w processes in Figure 7a−c with an enlargement for $\mathbf{2}_2$ in 7a) is based on the two-state model (Scheme 3), which assumes that the analyte after reorientation can dissociate only through the reverse of the reorientation (eq 1, where $\mathbf{2}_n$, $^{imp}\mathbf{2}_n$, $^{mic}\mathbf{2}_n$, and $^{reo}\mathbf{2}_n$ are defined as $\mathbf{2}_n$ in solution, $\mathbf{2}_n$ immobilized on the sensor chip with phosphate coating, $\mathbf{2}_n$ adsorbed as a micellar nanoparticle, and $\mathbf{2}_n$ after reorientation, respectively). If we define the surface concentrations of adsorbed species in the resonance units (*RU*), eqs 2−4 hold. The change in *RU* in the association and dissociation curves (a and c in the inset of Figure 7a) can be expressed as in eq 5. The maximal analyte binding capacity (ΔRU_{max}) is proportional to $[^{imp}\mathbf{2}_n]_{t=0}$ (eq 6). The rate constants were evaluated by means of a computer-aided least-squares curve-fitting method (BIAevaluation Ver. 3.0) under the boundary conditions of eq 7.

$$^{imp}\mathbf{2}_n + \mathbf{2}_n \underset{k_{d1}}{\overset{k_{a1}}{\rightleftharpoons}} {}^{imp}\mathbf{2}_n\cdot{}^{mic}\mathbf{2}_n \underset{k_{d2}}{\overset{k_{a2}}{\rightleftharpoons}} {}^{imp}\mathbf{2}_n\cdot{}^{reo}\mathbf{2}_n \tag{1}$$

$$-\mathrm{d}[^{imp}\mathbf{2}_n]/\mathrm{d}t = k_{a1}[^{imp}\mathbf{2}_n][\mathbf{2}_n] - k_{d1}[^{imp}\mathbf{2}_n\cdot{}^{mic}\mathbf{2}_n] \tag{2}$$

$$\mathrm{d}[^{imp}\mathbf{2}_n\cdot{}^{mic}\mathbf{2}_n]/\mathrm{d}t = k_{a1}[^{imp}\mathbf{2}_n][\mathbf{2}_n] - k_{d1}[^{imp}\mathbf{2}_n\cdot{}^{mic}\mathbf{2}_n] - k_{a2}[^{imp}\mathbf{2}_n\cdot{}^{mic}\mathbf{2}_n] + k_{d2}[^{imp}\mathbf{2}_n\cdot{}^{reo}\mathbf{2}_n] \tag{3}$$

$$\mathrm{d}[^{imp}\mathbf{2}_n\cdot{}^{reo}\mathbf{2}_n]/\mathrm{d}t = k_{a2}[^{imp}\mathbf{2}_n\cdot{}^{mic}\mathbf{2}_n] - k_{d2}[^{imp}\mathbf{2}_n\cdot{}^{reo}\mathbf{2}_n] \tag{4}$$

$$\Delta RU \propto [^{imp}\mathbf{2}_n\cdot{}^{mic}\mathbf{2}_n] + [^{imp}\mathbf{2}_n\cdot{}^{reo}\mathbf{2}_n] \tag{5}$$

$$\Delta RU_{max} \propto [^{imp}\mathbf{2}_n]_{t=0} \tag{6}$$

$$[^{imp}\mathbf{2}_n\cdot{}^{mic}\mathbf{2}_n]_{t=0} = [^{imp}\mathbf{2}_n\cdot{}^{reo}\mathbf{2}_n]_{t=0} = 0 \tag{7}$$

Acknowledgment. This work was supported by RFTF of Japan Society for the Promotion of Science (JSPS), by Grant-in-Aids for COE Research (no. 08CE2005), for Scientific Research on Priority Areas (no. 10134227), and for Scientific Research (no. 13490021) from the Ministry of Education, Science, Sports, and Culture, Japan, and also by CREST of Japan Science and Technology Corporation (JST). We are grateful to Mr. S. Aita of JEOL for measurements of TEM images of compound $\mathbf{2}_2$.

JA0275663